ology and Toxicology
DOI 10.1007/7653_2015_43

Tumor Targeting by RGD-Grafted PLGA-Based Nanotheranostics Loaded with Paclitaxel and Superparamagnetic Iron Oxides

Fabienne Danhier, Pierre Danhier, Nathalie Schleich, Chrystelle Po, S. Laurent, P. Sibret, C. Jérôme, V. Poucelle, Bernard Gallez, and Véronique Préat

Abstract

Theranostic nanoparticles have the potential to revolutionize cancer diagnosis and therapy. Many groups have demonstrated differential levels of tumor growth between tumors treated by targeted or untargeted nanoparticles; however, only few have shown in vivo efficacy in both therapeutic and diagnostic approach. Herein, we first develop and characterize dual-paclitaxel (PTX)/superparamagnetic iron oxide (SPIO)-loaded PLGA-based nanoparticles grafted with the RGD peptide, for a theranostic purpose. Second, we compare in vivo different strategies in terms of targeting capabilities: (1) passive targeting via the EPR effect, (2) active targeting of $\alpha_v\beta_3$ integrin via RGD grafting, (3) magnetic guidance via a magnet placed on the tumor, and (4) the combination of the magnetic guidance and the active targeting of $\alpha_v\beta_3$ integrin. In this chapter, we present the general flowchart applied for this project: (1) the polymer and SPIO synthesis, (2) the physicochemical characterization of the nanoparticles, (3) the magnetic properties of the nanoparticles, and (4) the in vivo evaluation of the nanoparticles for their therapeutic and diagnosis purposes. We employ the electron spin resonance spectroscopy and magnetic resonance imaging to both quantify and visualize the accumulation of theranostic nanoparticles into the tumors.

Keywords: PLGA-nanoparticles, SPIO, Paclitaxel, Cancer therapy, Magnetic resonance imaging, Tumor targeting, Nanotheranostic

1 Introduction

Theranostic nanoparticles have the potential to revolutionize cancer diagnosis and therapy. Theranostic refers to the combination of a therapeutic and a diagnostic agent in a same unique vector. Such a tool could be helpful in noninvasive assessment of the biodistribution, visualization of drug distribution, optimization of strategies, and prediction and real-time monitoring of therapeutic responses [1, 2].

Passive targeting is based on the so-called enhanced permeability and retention (EPR) effect [3]. This strategy relies on the

presence of fenestrations in the endothelium of tumor vessels, allowing the entry of nanoparticle into the tumor tissue. Moreover, the deficiency of the lymphatic system in tumor tissue prevents the recapture of these nanoparticles leading to a retention effect [3–5]. *Active targeting* consists in coupling a ligand to the surface of nanoparticles that can interact with its receptor at the target cell site [6, 7]. Although angiogenesis is a physiological process by which new blood vessels are formed, it is also at the root of tumor growth and metastasis. Since angiogenesis is controlled by the endothelial cells, it is of great interest to target tumor endothelial cells. $\alpha_v\beta_3$ is an adhesion integrin overexpressed at the surface of the endothelial cells of neo-angiogenic vessels involved in the angiogenic process. Its expression is correlated with the malignancy of tumor. Moreover, $\alpha_v\beta_3$ is also overexpressed at the surface of many tumor cells. Numerous studies have shown that the tripeptide arginine–glycine–aspartic acid (RGD) was able to bind preferentially to particular $\alpha_v\beta_3$ integrin [6, 8]. More recently, *magnetic drug targeting* has been studied. In this approach, magnetic nanoparticles are guided to tumor site using magnetic fields [9].

We hypothesized that the combination of both active strategy and magnetic guidance could enhance theranostic nanoparticle concentration into the tumor tissue leading, therefore, to a better anticancer efficacy (therapeutic purpose) and increased contrast enhancement in magnetic resonance imaging (MRI) (diagnosis purpose).

In this study, we aimed at developing RGD-grafted PEGylated PLGA-based nanoparticles as an effective nanocarrier for dual encapsulation of anticancer drug, paclitaxel (PTX), and small paramagnetic iron oxides (SPIO) for a theranostic purpose (Fig. 1). Hence, SPIO were prepared by the coprecipitation technique and were encapsulated in PLGA-based nanoparticles. The physicochemical properties of nanoparticles were characterized by different techniques such as transmission electron microscopy (TEM), dynamic light scattering (DLS) method, and electron spin resonance (EPR) spectroscopy. Their magnetic properties were evaluated using relaxometry and magnetic resonance imaging (MRI). Finally, we aimed at evaluating the combination of the two targeting strategies (active targeting and magnetic targeting) in vivo using two complementary techniques: (1) the ESR spectroscopy [10] and (2) the 11.7 T MRI [11].

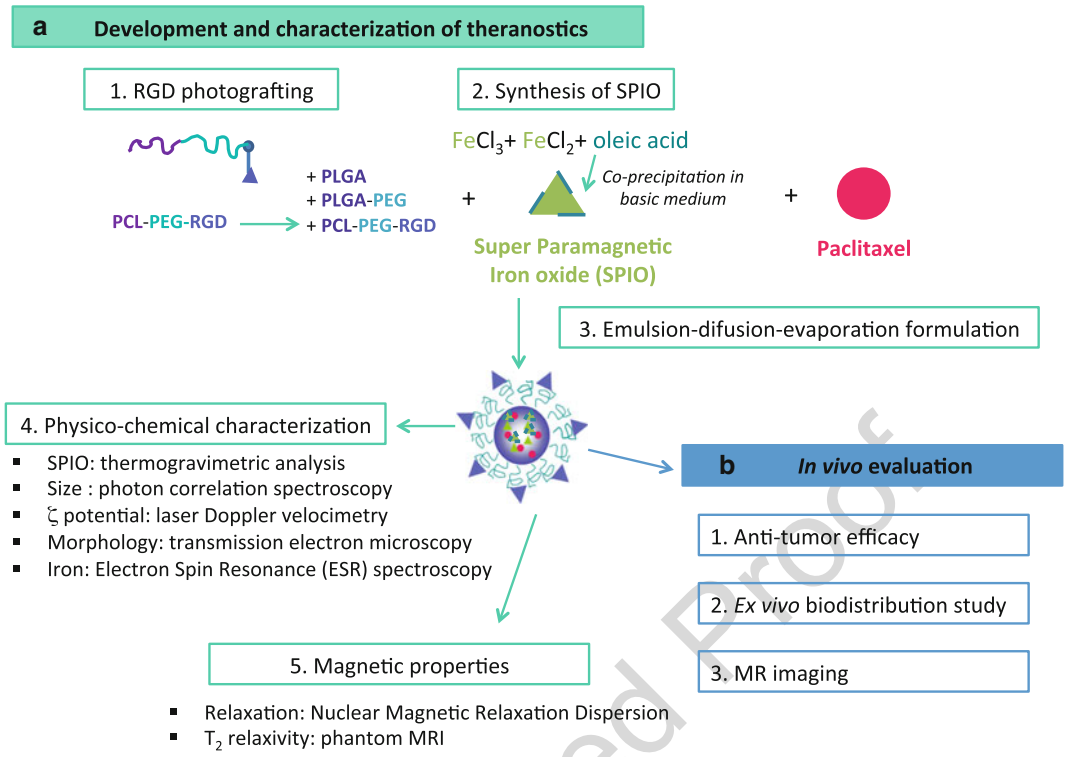

Fig. 1 Experimental flowchart of the current project highlighting the two main objectives: (**a**) the development and the characterization of nanotheranostics and (**b**) the in vivo evaluation to demonstrate the benefit of the combination of the active targeting and the magnetic guidance for both therapeutic and imaging purposes

2 Materials

1. Iron(II) chloride, Sigma-Aldrich (St. Louis, MO, USA).
2. Iron(III) chloride, Sigma-Aldrich (St. Louis, MO, USA).
3. Oleic acid, Sigma-Aldrich (St. Louis, MO, USA).
4. Nitrogen-gas.
5. Tetramethylammonium 11-aminoundecanoate, Sigma-Aldrich (St. Louis, MO, USA).
6. PCL-b-PEG (MW = 13,100–5000), synthesized by ring-opening polymerization using triethylaluminum as the catalyst [12].
7. O-succinimidyl 4-(p-azidophenyl) butanoate, Sigma-Aldrich (St. Louis, MO, USA).
8. GRGDS, NeoMPS (Strasbourg, France).
9. PTX, Sigma-Aldrich (St. Louis, MO, USA).

10. Poly(lactic-co-glycolic acid) (PLGA, lactide/glycolide molar ratio of 50:50 MW: 7000–17,000), Sigma-Aldrich (St. Louis, MO, USA).
11. PLGA-*b*-PEG (MW = 10,040–4600) was synthesized as previously described [13].
12. PVA: Polyvinylalcohol (MW = 30–70 kDa), Sigma-Aldrich (St. Louis, MO, USA).
13. Sonicator: Digital Sonifier, Branson (Danbury, USA).
14. 1.2 μm filters, Acrodisc 32 mm Syringe filter with 1.2 μm Supor membrane, Pall, Life Sciences (Zaventem, Belgium).
15. Thermogravimetric analysis (TGA): TA Instrument Q500 model (USA).
16. Transmission electron microscopy (TEM): Philips CM 100, equipped with a Megaview G2 camera (Andover, USA).
17. Malvern Nano ZS, Malvern instruments (UK).
18. Bruker EMX ESR spectrometer, Bruker Biospin GmBh (Germany).
19. Inductively coupled plasma mass spectroscopy (ICP-MS), Agilent 7500ce instrument.
20. High-performance liquid chromatography (HPLC), Agilent 1100 series, Agilent Technologies (USA). The column used was a CC 125/4 Nucleodur 100-5 C18, Macherey-Nagel (Bethlehem, USA).
21. Fast Field Cycling Relaxometer, Stelar (Mede, Italy).
22. Minispec spin analyzers, Bruker (Karlsruhe, Germany).
23. SPIO, BioPAL (Worcester, UK).
24. 11.7 T animal Biospec MR system, Bruker Biospec (Ettlingen, Germany).
25. 1.1 T neodyme-iron-bore external magnet, Webcraft GmbH (Uster, Switzerland).
26. Isoflurane, Abbott (Ottignies, Belgium).
27. Ketamine (Ketalar®) and Xylazine, Sigma-Aldrich (St. Louis, MO, USA).
28. CT26 cells, ATCC (Manassas, USA).
29. Freeze-dryer, Labconco (Kansas City, USA).
30. Haematocrit capillaries, ref 910 0175, Hirschmann Labor-geräte (Eberstadt, Germany).
31. Haematocrit sealing compound, Cat. No. 7495 10, Brand GmbH (Wertheim, Germany).
32. 18G needle, ref 304622, BD Microlance (Le Pont de Claix, France).

3 Methods

The methods described next follow the chronological steps of our experiment flowchart for the development of the PLGA-based nanotheranostics, shown in Fig. 1, and comprise (1) the synthesis of SPIO, (2) the photografting of PCL-b-PEG with the RGD peptide, (3) the preparation of the RGD-grafted PLGA-based nanoparticles, (4) the physicochemical characterization of the nanoparticles, and (5) the evaluation of the magnetic properties of the nanoparticles.

After that, the combination of the two strategies (active targeting + magnetic targeting) will be evaluated in vivo: (1) antitumor efficacy, (2) ex vivo biodistribution study, and (3) MR imaging.

3.1 Development of the PLGA-Based Nanotheranostics

3.1.1 Synthesis of Superparamagnetic Iron Oxides Coated with Oleic Acid

1. Hydrophobic SPIO were synthesized using a classical coprecipitation technique of ferrous and ferric salts in alkaline medium. 10 mmol iron(III) chloride and 5 mmol iron(II) chloride were mixed together in 12 ml of a hydrochloride aqueous solution (HCl 1 M).
2. This solution was then added dropwise to an aqueous solution of NaOH 1 M containing 3.1 g of oleic acid with stirring on a magnetic stir plate for 20 min under a nitrogen-gas atmosphere at 80 °C.
3. The black precipitate was separated using a magnet, washed three times using absolute ethanol, and then dissolved in 50 ml of dichloromethane (DCM).
4. The solution was then placed in an ultrasonic bath for 10 min and centrifuged (4416 rcf, 10 min) to remove the undispersed residue.
5. Hydrophilic SPIO used as SPIO aqueous solution (SPIO sol) were also synthesized. 1 ml of DCM dispersion of SPIO coated with oleic acid (40 mg/ml) was added to a suspension of tetramethylammonium 11-aminoundecanoate in DCM (40 mg in 2 ml). After 24-h magnetic stirring, the precipitate was washed three times with DCM and dispersed in water [14].

3.1.2 Photografting of PCL-b-PEG with the RGD Peptide

1. PCL-b-PEG was solubilized in methylene dichloride or acetonitrile (40 ml/g) with the molecular clip: O-succinimidyl 4-(p-azidophenyl) butanoate (0.2 mmol/g), and the solution was cast on clean plates (1 ml per plate).
2. After solvent evaporation, the polymer was dried under vacuum to constant weight and was removed from the plates as shaving.
3. The polymer sample was irradiated at 254 nm in a quartz flask under an argon atmosphere for 20 min, using a homemade

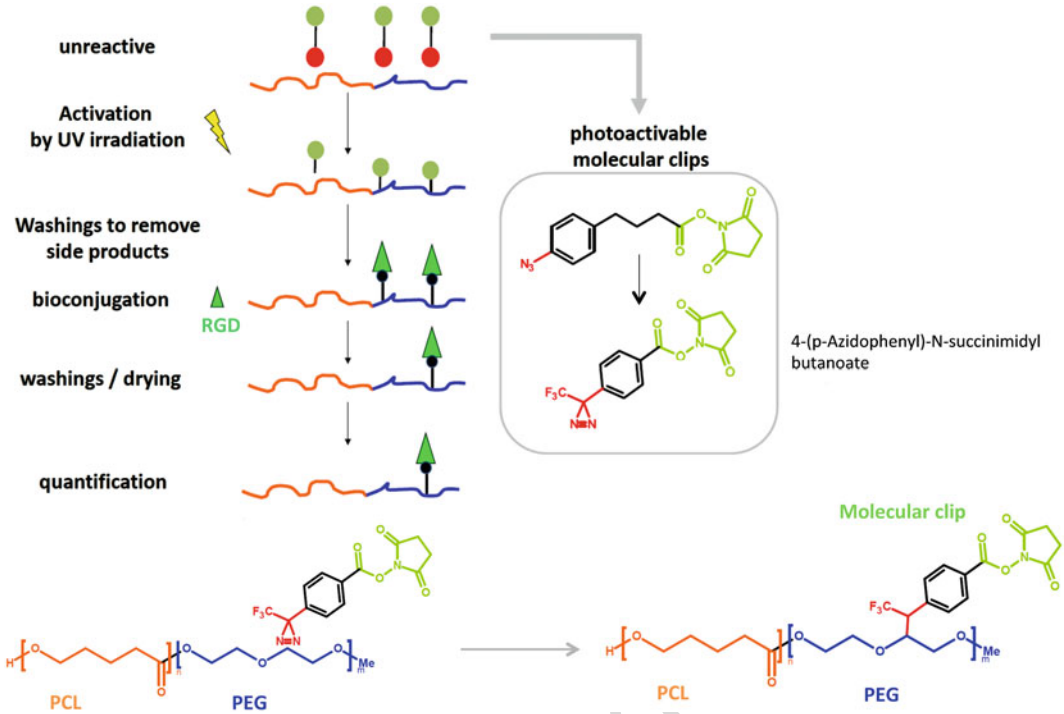

Fig. 2 Schematic representation of the RGD peptide grafting on the PCL-b-PEG copolymer [12]

reactor (rotating quartz flask of 15 ml; 3 UV lamps of 8 W placed at a distance of 4.5 cm).

4. The samples were washed (to remove unreacted arylazide and nonfixed reagent) with isopropanol:ethyl acetate (19:1, v/v) (80 ml/g; three times) and dried under vacuum. The "activated" polymer was immersed in 1 mM solution of the ligand GRGDS (80 ml/g) in phosphate buffer (0.1 M): acetonitrile (1:1, v/v) at pH 8 and shaken for 24 h at 20 °C.
5. The peptide solution was removed by suction and the sample was then washed three times with 5 mM HCl, five times with deionized water, shaken overnight in deionized water, rinsed with MeOH, and dried under the vacuum at 40 °C to a constant weight (Fig. 2) [15].

3.1.3 Preparation of RGD-Grafted PLGA-Based Nanoparticles Loaded with SPIO and Paclitaxel

RGD-grafted nanoparticles loaded with SPIO and PTX (SPIO/PTX-RGD-NP) were prepared by an emulsion-diffusion-evaporation method [14]. Chemical description of the polymers included in the formulations is illustrated in Table 1.

1. PLGA (14 mg/ml), PLGA-PEG (3 mg/ml), and PCL-PEG-RGD (3 mg/ml) were dissolved in 2 ml DCM containing SPIO (Fe concentration: 15 mg/ml) and PTX (3 mg).

Table 1
Chemical description of the polymers included in the formulations

Polymer	Mn (SEC) g/mol[a]	Mn (NMR) g/mol polyester-PEG	Mol % glycolidel[b]
PLGA	7000–17,000	–	50
PLGA-b-PEG	–	10,004–4600	26
PCL-b-PEG	22,400	13,100–5000	–

[a]Polystyrene calibration
[b]Determined by NMR by the following formula: $((I_{4.7}/2)/(I_{5.2} + I_{4.7}/2)) \times 100$, where $I_{4.7}$ is the signal intensity of the glycolide unit at 4.7 ppm ($CH_2OC{=}O$) and $I_{5.2}$ is the signal intensity of the lactide unit at 5.2 ppm ($CH(CH_3)OC{=}O$)

2. This organic solution was then added to an aqueous solution (4.5 ml) containing 3 % (p/v) PVA and emulsified using a vortex for 2 min followed by sonication (2 × 30 s, 50 W).
3. The mixture was then added dropwise and under magnetic stirring into an aqueous solution containing 1 % PVA and stirred overnight to evaporate the organic solvent. Some considerations around this procedure are gathered in **Note 1**.
4. To remove the non-encapsulated drug and the residual PVA, the suspension was filtered (1.2 μm) and washed three times with water using ultracentrifugation (11,000 × *g*, 30 min, 4 °C) and suspended in 2 ml water.

As a control, we used exactly the same method while PCL-PEG-RGD was replaced by PCL-PEG.

3.1.4 Physicochemical Characterization of Nanotheranostics

1. The coating percentage of SPIO with oleic acid was assessed by thermogravimetric analysis (TGA) on a TA Instrument Q500 model, under dry nitrogen flow, with a heating rate of 15 °C/min from RT to 600 °C, in an open platinum pan.
2. The hydrodynamic particle size and size polydispersity of nanoparticles were assessed by photon correlation spectroscopy, using a Malvern Nano ZS (Nano ZS, Malvern instruments, UK).
3. The morphology of the particles was achieved using transmission electron microscopy (TEM). TEM was carried out at a voltage of 100 kV. Samples for TEM experiments were prepared by spin coating a drop of nanoparticles in DCM on a carbon-coated TEM grid.
4. The zeta (ζ) potential of the nanoparticles was measured by laser Doppler velocimetry in KCl 1 mM with a Malvern Nano ZS at 25 °C.
5. Iron content was measured by ESR (Table 2) using a Bruker EMX ESR spectrometer operating at 9 GHz validated by inductively coupled plasma mass spectroscopy (ICP-MS) measurements.

Table 2
Comparison between the electron spin resonance (ESR) spectroscopy and the magnetic resonance imaging (MRI)

	ESR spectroscopy	MRI
Resonance method	Electron spin	Nuclear spin
Constant parameter	Constant frequency	Constant magnetic field
Frequency/magnetic field ratio	28 GHz/T	45 MHz/T
Relaxation time	Short (ns)	Long (ms)
B amplitude	0.34 T	11.7 T
Frequency	9.5 GHz	500 MHz
Energy level	Very high	High
Sensitivity	nM	μM

Some considerations around this procedure are gathered in **Note 2**. Typical parameters were selected for ESR measurements: 30 G modulation amplitude, 10.11 mW power, 3251 G center field, and 4000 G sweep width field. Measurements were performed at room temperature. Double integration (DI) of the first derivative of iron oxides ESR spectra (Bruker WINEPR software) was used to quantify signal intensity [16].

6. PTX content was determined using high-performance liquid chromatography (HPLC) with UV detection at 227 nm, after dissolution of the particles by acetonitrile. The mobile phase consisted of acetonitrile and water (70:30 v/v, respectively) at a rate of 1 ml/min. The column used was a CC 125/4 Nucleodur 100-5 C18. The drug loading was defined as the amount of drug (mg) loaded for 100 mg of polymer whereas the encapsulation efficiency was defined by the ratio of the encapsulated drug compared to the initial amount of drug [6].

3.1.5 Magnetic Properties of Nanotheranostics

1. Nuclear magnetic relaxation dispersion (NMRD) profiles were recorded at 37 °C on a fast-field cycling relaxometer over a magnetic field range from 0.01 to 40 MHz. Additional longitudinal (R_1) and transverse (R_2) relaxation rate measurements at 20 MHz and 60 MHz were, respectively, obtained on Minispec mq 20 and mq 60 spin analyzers. The fitting of the NMRD profiles by a theoretical relaxation model allows the determination of the crystal radius (r) and the specific magnetization (MS). The proton NMRD curves were fitted using data-processing software, including different theoretical models describing the nuclear relaxation phenomena [17].

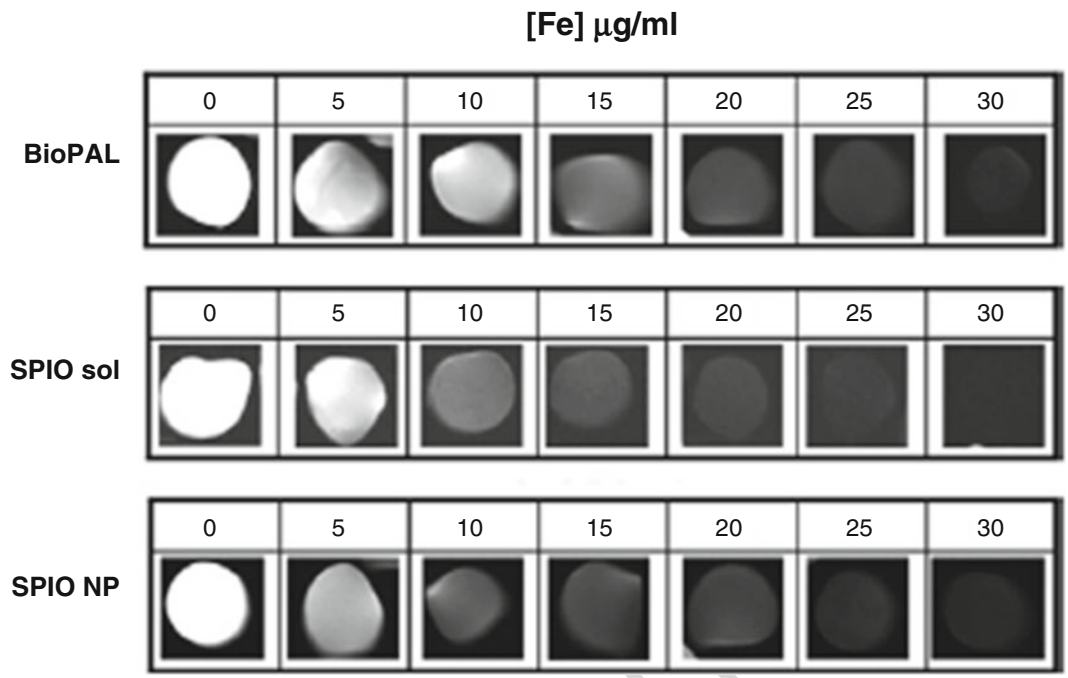

Fig. 3 T_2-weighted MR images (phantom MRI) of commercial SPIO (BioPAL, Worcester, UK), an aqueous suspension hydrophilic SPIO (SPIO sol), and SPIO-loaded nanoparticles (SPIO NP) as a function of Fe concentration (μg/ml, TE = 30 ms). Adapted from Ref. [14]

2. Various concentrations of SPIO in aqueous solution (SPIO sol) and PLGA-based nanoparticles loaded with SPIO (SPIO-NP) ranging from 0 to 30 μg/ml were investigated by T_2-weighted MRI to assess their T_2 enhancing capability. Commercial SPIO (BioPAL) were used as a reference at the same concentrations T_2 relaxivity was obtained using a 11.7 T animal Biospec MR system. Phantom MRI of SPIO-NP was carried out at various iron concentrations from 0 μg/ml to 30 μg/ml (0, 5, 10, 15, 20, 25, and 30 μg/ml) in 10 % gelatin using a T_2-weighted multi-slice multi-echo (MSME) sequence (Fig. 3). The imaging parameters were as follows: repetition time (TR) = 2500 ms, echo time (TE) = 30 ms, field of view (FOV) = 3.00 cm, and flip angle (FA) = 180.0°.

3.2 In Vivo Evaluation of the Combined Strategies: Active and Magnetic Targeting

3.2.1 Animal Tumor Model

CT26 colon carcinoma was chosen because of its sensitivity to PTX [18] and angiogenic properties [19]. CT26 colon carcinoma cells were inoculated subcutaneously in the right flank (for antitumor efficacy and biodistribution studies) or in the right leg (for MRI studies) of BALB/c mice (5×10^4 cells per mouse) depending on the experiment (*see* **Note 3**) [20]. For all the experiments, mice were divided into four groups: Group 1: control group (injected with PBS for in vivo antitumor efficacy

study and SPIO-loaded nanoparticles for ex vivo biodistribution and MRI), Group 2: mice treated by SPIO/PTX-NP grafted with RGD peptide (active targeting or RGD), Group 3: mice treated with SPIO/PTX-NP magnetic guided by placing a 1.1 T neodyme-iron-bore external magnet on the surface of the tumor during 1 or 4 h (magnetic guidance, MG) (*see* **Note 4**), and Group 4: mice treated with SPIO/PTX-NP grafted with RGD peptide using both magnetic and active targeting (RGD + MG).

PTX and Fe doses were 5 mg/kg and 27.1 mg/kg, respectively, for in vivo antitumor efficacy experiment and 2.5 mg/kg and 13.5 mg/kg for other experiments. For tumor inoculation, mice were anesthetized by intraperitoneal injections of a mixed ketamine (100 mg/kg) and xylazine (10 mg/kg). For in vivo MRI experiments, mice were maintained under anesthesia during the entire experiment using 1–2 % isoflurane inhalation in air.

3.2.2 Antitumor Efficacy

The effect of SPIO/PTX-RGD-NP on tumor growth was assessed by daily measurements of tumor volume with an electronic caliper. CT26 cells (5×10^4 cells per mouse) were injected subcutaneously in the right flank of the mice to allow easy and reproducible tumor volume measurements. Mice were randomly assigned to a treatment group when tumor reached a volume of 27 ± 5 mm^3. Treatments were injected trough the tail vein. Four groups were defined as aforementioned ($n = 6$): PBS, RGD, MG, and RGD+MG (PTX and Fe doses were 5 mg/kg and 27.1 mg/kg, respectively). In this experiment, the magnet was placed on the surface of the tumor during 4 h. The end point of the experiment was determined as the moment when tumor reached 600 mm^3. At this point, mice were sacrificed.

3.2.3 Ex Vivo Biodistribution Study by ESR Spectroscopy

The biodistribution of the different treatments was assessed using ESR spectroscopy (X-band) (*see* **Note 2**). CT26 cells (5×10^4 cells per mouse) were subcutaneously inoculated in the right flank of the mice. When tumor reached 50–100 mm^3 in volume, mice were randomly dispersed into four groups as aforementioned ($n = 6$): PBS, RGD, MG, and RGD + MG. For mice treated with magnetic guidance, the external magnet was maintained on the tumor until sacrifice. Treatments were injected in the tail vein of the mouse. 1 or 4 h posttreatment, mice were first taken a retro-orbital blood sample and were then sacrificed for dissection in order to remove liver, lungs, and tumor. Thereafter, samples were frozen in liquid nitrogen, dehydrated for 24 h in a freeze-dryer, crushed into a fine powder, weighed, and analyzed by ESR spectroscopy to determine iron concentration in each tissue.

3.2.4 In Vivo MR Imaging

For these experiments, CT26 cells (5×10^4 cells per mouse) were injected subcutaneously in the right leg of the mice to avoid respiratory artifacts (*see* **Note 3**). Mice were enrolled in the study when tumor reached 50–100 mm^3 in diameter (*see* **Note 5**). Three groups were defined ($n = 5$): RGD, MG, and RGD + MG. Each mouse was imaged before and 1 h after treatment injection in the tail vein in order to use each mouse as its own control.

MR experiments were performed using a 11.7 T Bruker Biospec horizontal MR System (Table 2). RF transmission and reception were achieved with a quadrature volume resonator (inner diameter 40 mm).

1. Mice were anesthetized by isoflurane inhalation 3 % in air and they were placed in an MRI-compatible cradle.
2. The breathing rate was assessed via a breathing pillow, placed under the thorax, and kept at 70 breaths/min by adjusting the isoflurane concentration. The body temperature was maintained at 37 °C by a warm waterbed and monitored using a rectal probe. Vital functions were monitored during the whole anesthesia period using SamPC Monitor (version 6.17, Small Animal Instruments Inc.).
3. Anatomical images of the mice were provided by T_2-weighted axial images acquired with a rapid acquisition with relaxation enhancement sequence (RARE; TR/TE: 2500/30 ms, RARE factor: 6, 10 slices non-contiguous with a gap of 0.08 mm, resolution: $125 \times 125 \times 800$ μm^3).
4. T_2 maps were acquired with the same geometry than the anatomical images using an MSME sequence (TR/TE: 2500/10 ms; 16 echoes).
5. Quantitative T_2 maps were calculated from the MSME multi-echo trains and assuming mono-exponential decays, using ImageJ (ImageJ version, 1.48 NIH).
6. The volume of interest (VOI) corresponding to the tumor volume was manually delineated on a slice-by-slice basis on the anatomical images acquired before and after treatment injection, for each animal. These VOIs were applied on corresponding maps to determine the T_2 values. Relative standard deviations (RSD) were calculated as RSD = SD/mean T_2, where SD is the standard deviation of the mean T_2 value. T_2-weighted images, obtained with different TE from MSME sequence, are illustrated in Fig. 4.

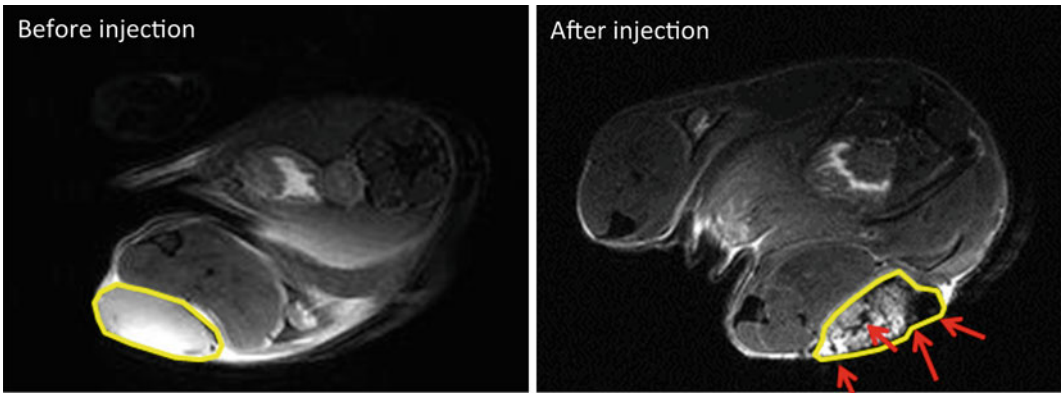

Fig. 4 T_2-weighted images, obtained from MSME sequence (TE = 10 ms) of CT26-tumor bearing mice pre-injection and 4 h after injection. Mice were treated with SPIO/PTX-NP grafted with RGD peptide using both magnetic and active targeting (RGD + MG). The position of dark region in tumor was pointed by *red-head arrows* ($n = 5$). Adapted from Ref. [20]

4 Notes

1. For the last step of the nanoparticle formulation: "The mixture was then added dropwise and under magnetic stirring into an aqueous solution containing 1 % PVA and stirred overnight to evaporate the organic solvent" (*see* section 3.1.3); it is important to note that (1) the mixture should be contained in a glass syringe with a 21 G needle. The size of the needle influenced the size and the polydispersity index of the nanoparticles; and (2) the mixture should be added dropwise in the vortex of the liquid created by the magnetic stirring. This step is also important for the size of the nanoparticles and to avoid aggregation of the nanoparticles (Fig. 5).
2. The iron oxide content of the nanoparticles was determined by ESR spectroscopy (also called electron paramagnetic resonance, EPR). ESR is a spectrometric technique that is used to study free radicals and (super) paramagnetic molecules. The ESR method was shown to be sensitive and specific for the iron oxide content determination in biological samples [16, 21]. SPIO present a typical broad ESR spectrum at room temperature that can be differentiated from free Fe^{+++} ion. Double integration (DI) of the first derivative ESR spectrum is used to quantify the amount of SPIO in a sample (Fig. 6). To obtain a linear relationship between the DI values of ESR spectra and the SPIO concentration, the baseline of ESR spectra must be flat. Otherwise, baseline corrections are needed to improve the accuracy of ESR measurements.

   Previously, ESR has already been described for studying iron oxide particles, mainly to characterize their physicochemical

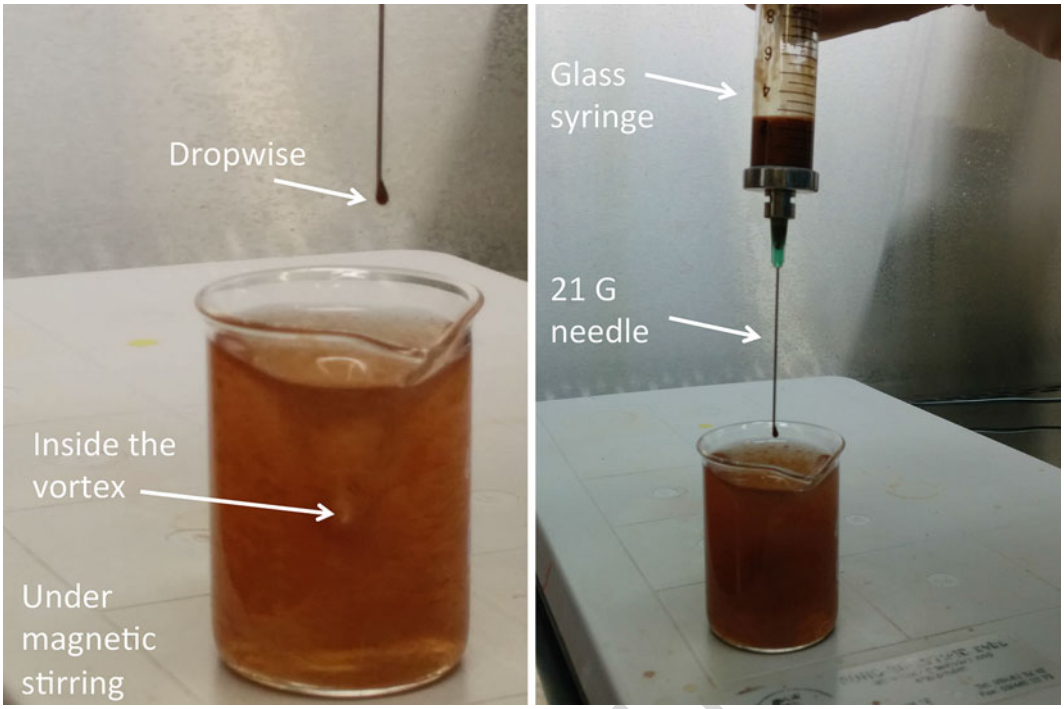

Fig. 5 Preparation of RGD-grafted PLGA-based nanoparticles loaded with SPIO and paclitaxel. The mixture was added dropwise with a glass syringe and a 23G needle under magnetic stirring into an aqueous solution containing 1 % PVA and stirred overnight to evaporate the organic solvent

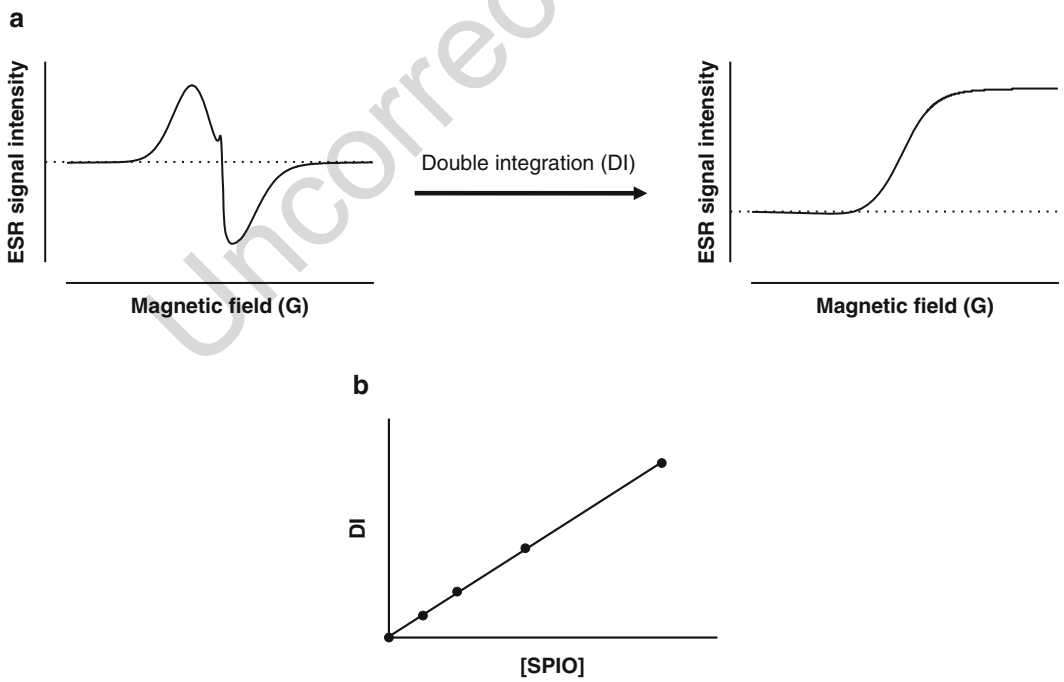

Fig. 6 Quantitative ESR. (**a**) Double integration (DI) of the first derivative of an SPIO ESR spectrum. For quantitative ESR, the baseline of acquired ESR spectra should be flat. (**b**) Linear relationship between DI values and the SPIO content in samples

properties or to measure their distribution in tissues after systemic injection [21]. For the characterization of new SPIO formulations using ESR spectroscopy, a calibration curve using several dilutions of iron oxides is mandatory to precisely determine the iron oxide content of samples. Of note, iron oxides used for the calibration must share similar physicochemical properties than those contained in the samples [16, 21]. For this reason, inductively coupled plasma mass spectroscopy (ICP-MS) was used to validate the ESR technique [16] (*see* section 3.1.4). Unlike ESR, ICP-MS is not specific for SPIO and measures the total iron content in samples [16, 21]. ESR was used in several studies to measure in vitro and ex vivo the iron oxide content in cells and rodent tissues such as the liver, the brain, the lungs, the kidneys, and tumor tissues, while ICP-MS cannot [21, 22].

For iron oxide quantification in aqueous solutions (Fig. 7), samples are drawn into 75 μL hematocrit capillaries. Capillary tubes are sealed using hematocrit sealing compound. Samples are next placed into ESR quartz tubes. In order to obtain reproducible ESR measurements (ESR spectrometer operating at 9.4 GHz), it is crucial to keep the exact same location of the samples in the ESR cavity (*see* section 3.1.4).

To quantify ex vivo the iron oxide content in rodent tissues (Fig. 8), sample freeze-drying is mandatory to minimize the non-resonant absorption of the electromagnetic radiation by

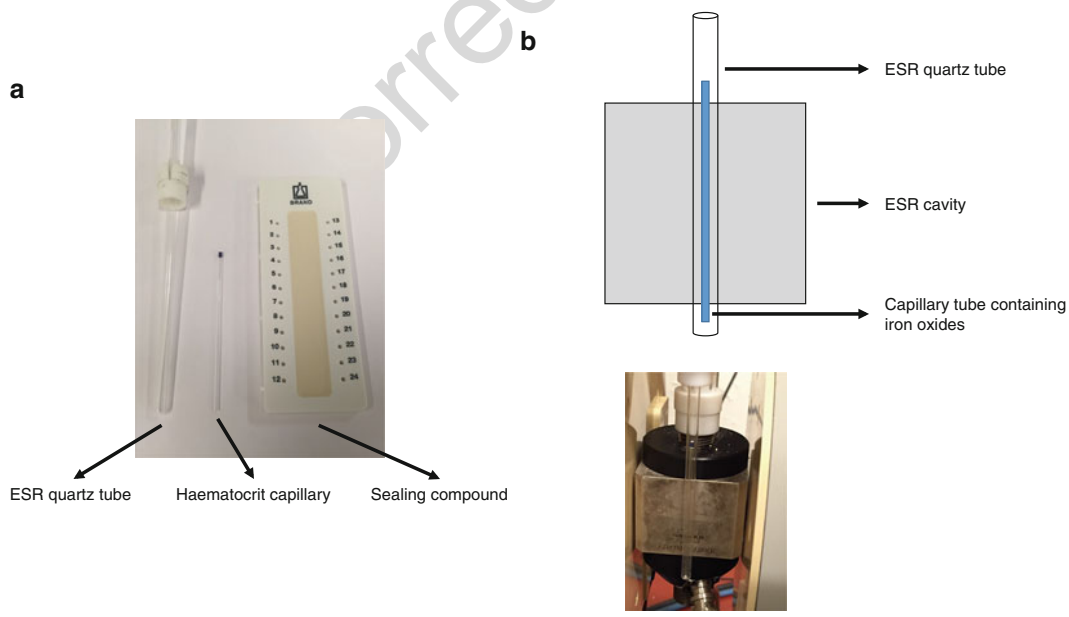

Fig. 7 ESR measurements of aqueous samples containing iron oxides. (**a**) Material needed for ESR measurements. (**b**) Schematic representation (*upper panel*) and picture (*lower panel*) of ESR tube positioning. The samples should always be placed at the same position in the center of the ESR cavity

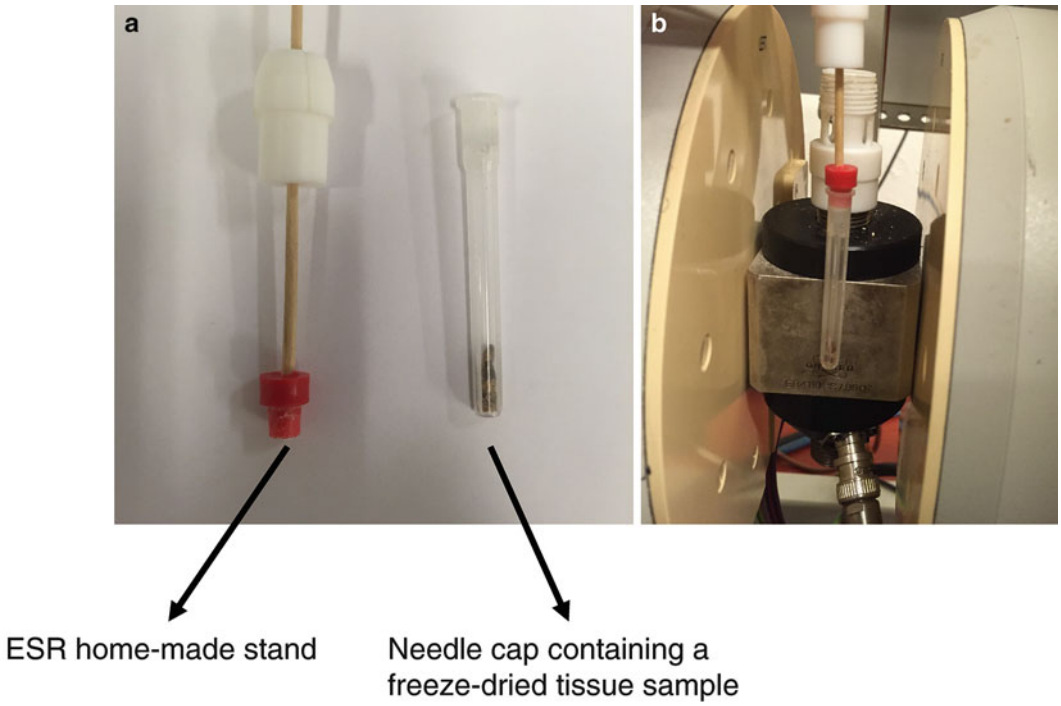

Fig. 8 Ex vivo ESR measurements of freeze-dried tissue samples containing SPIO. (**a**) Material needed for ESR measurements. (**b**) Picture showing a correct positioning of the sample in the center of the ESR cavity

the liquid water contained in tissues (*see* section 3.2.3). The freeze-dried sample, crushed into a fine powder, is weighed and then placed in the cap of an 18G needle. The cap containing the sample is next fixed to a homemade ESR stand. As already stated, the position of samples in the ESR cavity must be kept constant for all measurements in order to obtain reproducible data. For the SPIO calibration, liquid iron oxide standards are dispensed in caps of 18G needles, briefly centrifuged, and next heated for 72 h at 60 °C to remove the water. After iron oxide quantification, results are normalized to the dry weight of samples.

3. For antitumor efficacy and biodistribution studies, CT26 colon carcinoma was implanted subcutaneously in the right flank of mice (*see* sections 3.2.1 and 3.2.4). Volume of spheroidal tumor was measured as described previously using the formula $V = l \times w \times h$, where V = volume, l = length, w = width, and h = height [14, 23]. These external tumors can be daily measured using an electronic caliper. By contrast, for MRI studies, because of its localization, respiratory artifacts appeared, and correct acquisitions of tumors were impossible to perform. For this reason, we decided to change the localization of the tumor. We implanted thus CT26 tumor cells

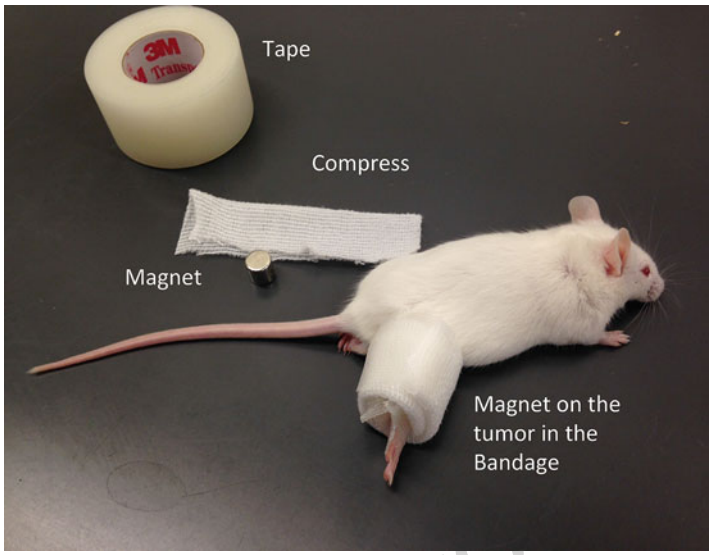

Fig. 9 Positioning in a bandage of a 1.1 T neodyme-iron-bore external magnet on the surface of the tumor during 1 or 4 h on CT26 tumor-bearing mice

subcutaneously in the right leg of mice. The size of the tumor was evaluated first using the electronic caliper and more precisely by MRI (*see* **Note 5**).

4. For the magnetic guidance of SPIO-loaded nanoparticles, use a 1.1 T neodyme-iron-bore external magnet on the surface of the tumor during 1 or 4 h (*see* section 3.2.1). Under anesthesia, a bandage was performed to avoid mice to remove their magnet. First, the magnet was maintained with compresses, avoiding injury. Second, the whole was fixed with a 3 M tape (Fig. 9).
5. As aforementioned in **Note 3**, for MRI studies, the size of tumors for the study might be between 50 and 100 mm^3. A first approximate measurement was performed using the electronic caliper. We observed that MRI results and associated RSD were impossible to compare due to the difference of tumor size of mice. Hence, before each MRI acquisition of a mouse, the volume of the tumor was measured and determined precisely, using the delimitation of the VOI, as explained in section 3.2.4.

Acknowledgment

This work is supported by grants from the Université catholique de Louvain (F.S.R.) and *Fonds National de la Recherche Scientifique* (F.R.S.-F.N.R.S.). F. Danhier is a Postdoctoral F.R.S.-F.N.R.S. Research Fellow. The funders had no role in study design, data collection and analysis, decision to publish, or preparation of the manuscript.

AU1

References

1. Janib SM, Moses AS, MacKay JA (2010) Imaging and drug delivery using theranostic nanoparticles. Adv Drug Deliv Rev 62:1052–1063
2. Lammers T, Kiessling F, Hennink WE et al (2010) Nanotheranostics and image-guided drug delivery: current concepts and future directions. Mol Pharm 7:1899–1912
3. Maeda H (2001) The enhanced permeability and retention (EPR) effect in tumor vasculature: the key role of tumor-selective macromolecular drug targeting. Adv Enzyme Regul 41:189–207
4. Danhier F, Feron O, Preat V (2010) To exploit the tumor microenvironment: passive and active tumor targeting of nanocarriers for anti-cancer drug delivery. J Control Release 148:135–146
5. Taurin S, Nehoff H, Greish K (2012) Anticancer nanomedicine and tumor vascular permeability; where is the missing link? J Control Release 164:265–275
6. Danhier F, Vroman B, Lecouturier N et al (2009) Targeting of tumor endothelium by RGD-grafted PLGA-nanoparticles loaded with paclitaxel. J Control Release 140:166–173
7. Danhier F, Le Breton A, Preat V (2012) RGD-based strategies to target alpha(v) beta(3) integrin in cancer therapy and diagnosis. Mol Pharm 9:2961–2973
8. Garanger E, Boturyn D, Coll JL et al (2006) Multivalent RGD synthetic peptides as potent alphaVbeta3 integrin ligands. Org Biomol Chem 4:1958–1965
9. Cole AJ, Yang VC, David AE (2011) Cancer theranostics: the rise of targeted magnetic nanoparticles. Trends Biotechnol 29:323–332
10. Radermacher KA, Beghein N, Boutry S et al (2009) In vivo detection of inflammation using pegylated iron oxide particles targeted at E-selectin: a multimodal approach using MR imaging and EPR spectroscopy. Invest Radiol 44:398–404
11. Radermacher KA, Magat J, Bouzin C et al (2012) Multimodal assessment of early tumor response to chemotherapy: comparison between diffusion-weighted MRI, 1H-MR spectroscopy of choline and USPIO particles targeted at cell death. NMR Biomed 25:514–522
12. Pourcelle V, Freichels H, Stoffelbach F et al (2009) Light induced functionalization of PCL-PEG block copolymers for the covalent immobilization of biomolecules. Biomacromolecules 10:966–974
13. Zweers ML, Engbers GH, Grijpma DW et al (2004) In vitro degradation of nanoparticles prepared from polymers based on DL-lactide, glycolide and poly(ethylene oxide). J Control Release 100:347–356
14. Schleich N, Sibret P, Danhier P et al (2013) Dual anticancer drug/superparamagnetic iron oxide-loaded PLGA-based nanoparticles for cancer therapy and magnetic resonance imaging. Int J Pharm 447:94–101
15. Pourcelle V, Devouge S, Garinot M et al (2007) PCL-PEG-based nanoparticles grafted with GRGDS peptide: preparation and surface analysis by XPS. Biomacromolecules 8:3977–3983
16. Danhier P, De Preter G, Boutry S et al (2012) Electron paramagnetic resonance as a sensitive tool to assess the iron oxide content in cells for MRI cell labeling studies. Contrast Media Mol Imaging 7:302–307
17. Laurent S, Bridot JL, Elst LV et al (2010) Magnetic iron oxide nanoparticles for biomedical applications. Future Med Chem 2:427–449
18. Yang HW, Hua MY, Liu HL et al (2012) An epirubicin-conjugated nanocarrier with MRI function to overcome lethal multidrug-resistant bladder cancer. Biomaterials 33:3919–3930
19. Lyons JA, Sheahan BJ, Galbraith SE et al (2007) Inhibition of angiogenesis by a Semliki Forest virus vector expressing VEGFR-2- reduces tumour growth and metastasis in mice. Gene Ther 14:503–513
20. Schleich N, Po C, Jacobs D et al (2014) Comparison of active, passive and magnetic targeting to tumors of multifunctional paclitaxel/SPIO-loaded nanoparticles for tumor imaging and therapy. J Control Release 194:82–91
21. Danhier P, De Preter G, Magat J et al (2014) Multimodal cell tracking of a spontaneous metastasis model: comparison between MRI, electron paramagnetic resonance and bioluminescence. Contrast Media Mol Imaging 9:143–153
22. Danhier P, Magat J, Leveque P et al (2015) In vivo visualization and ex vivo quantification of murine breast cancer cells in the mouse brain using MRI cell tracking and electron paramagnetic resonance. NMR Biomed 28:367–375
23. Na HS, Lim YK, Jeong YI et al (2010) Combination antitumor effects of micelle-loaded anticancer drugs in a CT-26 murine colorectal carcinoma model. Int J Pharm 383:192–200

Author Queries

Chapter No.: 43

Query Refs.	Details Required	Author's response
AU1	Note that Refs. [6] and [17] are identical, so we have deleted the latter reference and renumbered the remaining references; please confirm.	